Indian Journal of Pure & Applied Physics
Vol. 60, September 2022, pp. 727-733
DOI: 10.56042/ijpap.v60i9.64411

High-Performance of Star-Photonics Crystal Fiber Based on Surface Plasmon Resonance Sensor

Dedi Irawan[a*], Khaikal Ramadhan[b], Saktioto[b], Fitmawati[c], Bambang Widiyatmoko[d] & Dwi Hanto[d]

[a]Department of Physics Education, Faculty of Teacher Training and Education, Universitas Riau, Pekanbaru, 28293, Indonesia

[b]Department of Physics, Mathematics and Natural Sciences, Universitas Riau, Pekanbaru, 28293, Indonesia

[c]Department of Biology, Mathematics and Natural Sciences, Universitas Riau, Pekanbaru, 28293, Indonesia

[d]Research Center of Physics, National Research and Innovation Agency PUSPIPTEK Serpong, South Tangerang, 15314, Indonesia

Received 11 July 2022; accepted 17 August 2022

Photonic Crystalline (PCF)-based SPR (Surface Plasmon Resonance) sensors continue to develop and achieve good performance, but in previous studies, PCF-SPR only has a small refractive index range detection, complex geometric structure, and low sensitivity. In this paper, we investigate the performance of the Star-shaped PCF-SPR sensor (S-PCF-SPR) in detecting the refractive index of the analyte. We performed numerical simulations using the finite element method (FEM) based on COMSOL Multiphysics version 5.6. It was found that S-PCF-SPR can detect analytes in a wide refractive index range from 1.3 to 139 RIU. S-PCF-SPR has a maximum wavelength sensitivity of 12000 nm/RIU, and the sensor resolution resulting from S-PCF-SPR 5.4 × 10^{-5}. These results indicate that the S-PCF-SPR can be used as a sensor for sensitive analyte sensing applications and has good sensor resolution.

Keywords: Photonics Crystal; Surface Plasmon Resonance; High-Performance; Refractive index

1 Introduction

Sensing technology continues to develop until today. Surface plasmon resonance (SPR) sensors show excellent performance in environmental sensings such as temperature sensing[1,2], analyte refractive index[3-5], and magnetic field[6,7]. SPR is not only used in single parameter sensing[8] but also used in simultaneous sensing of temperature and refractive index[9,10], magnetic field and temperature[11,12], pH and refractive index[13], temperature and strain[14]. The combined SPR sensor based on photonic crystal fiber is a new and flexible type of sensor, this type of sensor has several unique advantages in measurement such as high birefringence[15,16], very fast sensing[17], low transmission loss and not susceptible to the damage of electromagnetic waves[18], very high sensitivity[19,20]. plasmonic material dissociated on PCF provides a plasmon resonance phenomenon in the device so that it can be used to detect analytes that can be used in the medical area[21,22].

The most common plasmonic materials used in coating PCF are gold[23-25], silver[26], copper[27], titanium[28]. When plasmonic material and dielectric material meet with electromagnetic waves, it will bring up surface plasmon (SP) due to electron oscillation on the surface of plasmonic material[18], so PCF-SPR becomes a popular sensor device with its advantages such as small size[29], can detect more than one analyte[30,31], and multi-channels[32,33].

The SPR technique is popularly used in sensing because of its accuracy and sensitive sensing performance and can detect the refractive index of the analyte in the order of 0.01 of the refractive index changes[17]. In the phase-matching condition, the energy transferred from the core to the plasmon mode causes a shift in the peak of the confirmation loss. Confinement loss is the loss of space generated by the air around the PCF core[18]. It was also found that the confinement loss peak shifted as the refractive index of the analyte changed so that this event would provide information related to the type of analyte included in the PCF-SPR[34]. The PCFs used in the SPR technique are usually made of silica[35], graphene[27], TOPAS[36], Zeonex[37]. Among the many materials proposed by the researchers, PCF-SPR with fused silica material gave the best performance.

Many researchers have reported various types of PCF-SPR geometric structures ranging from hexagonal[17], octagonal[38], D-shape[15], and PCF-SPR resembling the Marcedes Benz logo[39]. Other

*Corresponding authors: (Email: Dedi.irawan@lecturer.unri.ac.id)

researchers also proposed PCF-SPR based on sensory systems such as internal sensing and external sensing[33]. some researchers have also reported the results of the performance of the design as reported by Meng et al obtained a sensitivity of 3330 nm/RIU and can detect the refractive index in the range 1.35 – 1.4 RIU[40], the study reported by Danlard *et al*. in 2022 obtained PCF-SPR can detect the refractive index in the range 1.4-1.46 RIU and obtained a maximum design wavelength sensitivity of 3000 nm/RIU[41], other researchers also reported that PCF-SPR with silica and multiple-hole geometry strictures can detect refractive index in the range 1.25-1.3 RIU obtained maximum wavelength sensitivity of 1932 nm/RIU[42], recently Bahloul *et al*. reported that PCF-SPR obtained a maximum sensitivity of 4100 nm/RIU and could detect refractive index in the range 1.38 – 1.4 RIU[43], and Zhang et al. reported that the D-shaped PCF-SPR can detect analytes in the refractive index range of 1.33 – 1.34 RIU with a sensitivity of 1371 nm/RIU[44]. However, from all that recommended by previous researchers, the geometric structure is difficult to fabricate, the refractive index range is still small and the sensitivity is low.

In this paper, we investigate the S-PCF-SPR with a hexagonal 3-layers star-shaped geometric structure. The performance factors of the sensor being investigated are maximum wavelength sensitivity, wide refractive index sensing range, amplitude sensitivity, and sensor resolution. The research was conducted using the finite element method based on COMSOL Multiphysics 5.6.

2 Geometri Structure Purposed Sensor

In this paper, we investigate the star-shaped PCF-SPR design (S-PCF-SPR) using the finite element method (FEM) using COMSOL Multiphysics version 5.6. In this investigation, PCF uses fused silica which can be defined by the sellmeier equation as in Eq 1. Fused silica is the most commonly used PCF material, and it is reported to have the best performance when compared to other materials such as TOPAS, Zeonex etc. The sellmeier equation can be used in defining the fused silica material in the S-PCF-SPR design. The distribution of the refractive index for silica materials can be seen in Eq 1.

$$n(\lambda)=\sqrt{1+\frac{0.696\lambda^2}{\lambda^2-0.0047}+\frac{0.408\lambda^2}{\lambda^2-0.014}+\frac{0.897\lambda^2}{\lambda^2-97.934}} \quad \text{... (1)}$$

Where n is the refractive index of silica for each particular wavelength, λ is the wavelength that illuminates the surface of the S-PCF-SPR. The plasmonic material used to elicit the SPR effect on the PCF, the plasmonic material used in this study is gold, gold is chemically more stable than the environment but shows a wide resonance peak and this will harm the components. The drude-Lorentz model is used to calculate the dielectric constant of gold which can be shown in Eq 2.

$$\varepsilon_{au}=\varepsilon_{\infty}-\frac{\omega_D^2}{\omega\left(\omega+j\gamma_D\right)}-\frac{\Delta\varepsilon\Omega_L^2}{\left(\omega^2-\Omega_L^2\right)+j\Gamma_L\omega} \quad \text{... (2)}$$

With Au being the gold permittivity value, and high-frequency permittivity with a value of 5.9673, then is the plasma frequency, where D is the dumping frequency and D is the plasmon frequency which numerically has a value of 31.84π THz and 4227.2π THz and the oscillator power with symbol L = 1300.14π THz, and the spectral width is L = 209.72π THz.

PCF that has air holes around the surface will cause loss when passing through the surface. This confinement loss can be defined as Eq 3.

$$L_c\left(dB/cm\right)=\left(\frac{4\pi f}{c}\right)\mathrm{Im}\left(n_{eff}\right)\times 10^4 \quad \text{... (3)}$$

Where Lc is the material confinement loss, with a value of 3.14, f = frequency, n_{eff} is the effective refractive index, and c is the speed of light. Meanwhile, S-PCF-SPR performance factors such as wavelength sensitivity can be defined in Eq 4.

$$S_\lambda\left(nm/RIU\right)=\Delta\lambda_{peak}/\Delta n \quad \text{... (4)}$$

Wavelength sensitivity shows how big the shift in the wavelength of the peak loss is for each change in the analyte's refractive index. A large shift for a small change in the refractive index of the analyte will show components that are ultra-sensitive and have high performance in differentiating changes in the refractive index of the analyte. Wavelength sensitivity also shows the difference in peak loss at a certain wavelength divided by the difference in the sensing refractive index. Furthermore, the sensor resolution is mathematically shown by Eq 5. The proposed sensor geometry structure is shown in Fig. 1. The sizes d1, d2, and d3 are d/3, d/2.5, and d/2, respectively, with a d value of 1.4 μm

$$R=\frac{\partial n_a\times\partial\lambda_{\min}}{\partial\lambda_{peak}}(RIU) \quad \text{... (5)}$$

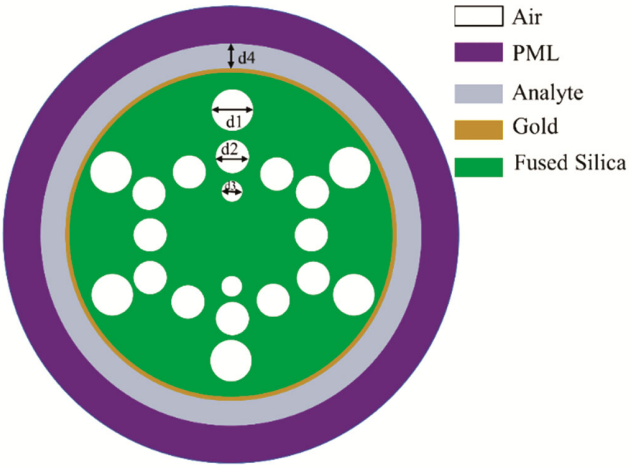

Fig. 1 — The geometrical structure of the proposed PCF-SPR.

3 Results and Discussion

After doing the simulation using the finite element method assisted by COMSOL Multiphysics Version 5.6. The FEM method is used to evaluate the geometric structure and analyze the performance of the PCF-SPR sensor such as sensitivity, loss confinement, amplitude sensitivity, sensor resolution, and FWHM (Full-width Half Maximum). Simulation is done by selecting the analysis mode with the electromagnetic frequency domain (EWFD) on COMSOL. The geometrical structure of PCF is arranged as shown in Fig. 1. PCF is defined as a fused silica material following equation 1. And the plasmonic material used in this research is gold based on the drude-Lorentz model based on equation 2. After the material definition is carried out, the simulation process is then carried out by investigating the mode at the refractive index of 1.46 RIU. Furthermore, the distribution of the electromagnetic field for the SPP mode and the polarization of the x-axis and y-axis is obtained as shown in Figs 2, 2(a) for SPP mode, 2(b) x-pol, and 2(c) y-pol.

PCF-SPR has an analyte layer of d4 = 0.5 µm outside the gold layer with a thickness of 40 nm, then on the outermost layer, the design is limited by a PML (Perfectly Matched Layer) layer with a thickness of 1 µm which will limit the distribution of the electromagnetic field on the core surface. and sensor cladding.

In Fig. 2 the distribution of the electric field around the PCF-SPR surface. The refractive index of the analyte defined in the distribution of Fig. 2 is 1.3 RIU. for further variation of the analyte with different refractive indices. It was found that the PCF-SPR

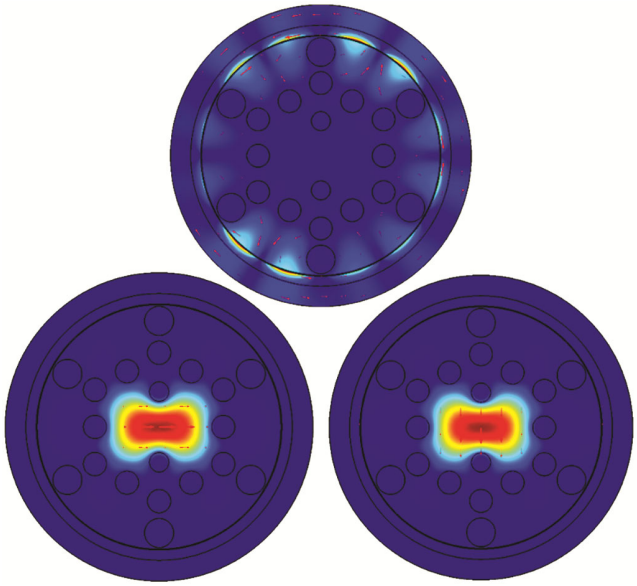

Fig. 2 — Electric field distribution on the PCF-SPR surface (a) SPP mode, (b) X-polarization (c) Y-polarization, with a gold thickness of 40 nm.

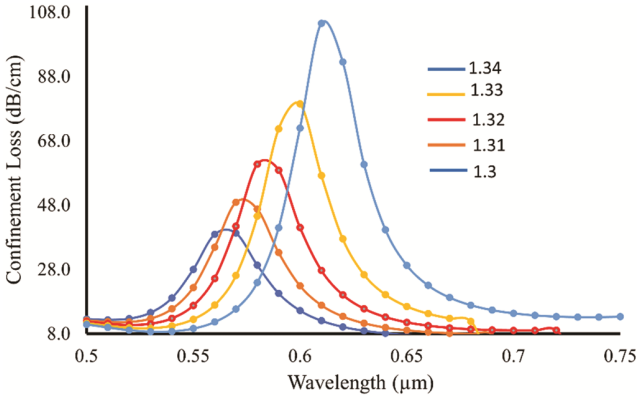

Fig. 3 — Confinement loss shift for each change in the refractive index of the analyte in the range 1.3 – 1.34 RIU.

design can detect analytes in the range of the basic index of 1.3 – 1.39 RIU, this range is broad compared to previously reported studies[43-45]. When the analyte has a refractive index of 1.4 RIU, the resonant wavelength is not found in this design, then the confinement loss has no peak value. The shift in the confinement loss peak in the design for each refractive index in the range 1.3 – 1.39 RIU can be seen in Fig. 3.

3.1 Confinement loss peak shift for each change in refractive index

In this section, the PCF-SPR sensitivity test is carried out in the refractive index range of 1.3 to 1.39 RIU. This sensing range is much wider when compared to the sensor components proposed by

other researchers[39-41]. In this case, we observe a confinement loss for each change in the analyte's refractive index of 0.01 RIU. We find that a large analyte refractive index will give a large confinement loss value and vice versa. This is due to an increase in the coupling in the design. In Fig. 3 we show only the surface polarization on the x-axis (x-pol), we find that the y-pol does not show a consistent value when sensing the analyte. So it is not used as a reference in sensing analytes. Next, calculate the confinement loss value for each particular refractive index by following equation 3. The effective refractive index is found for each wavelength and transformed into the imaginary value of each refractive index. So that the confinement loss shift for each refractive index is obtained as shown in Fig. 3. At the refractive index of 1.3 RIU, the confinement loss peak is 39.3 dB/cm and is known to be at a wavelength of 570 nm, then the refractive index is increased by 0.01, and the confinement loss peak is 48.9. dB/cm which is also at a wavelength of 570 nm. However, from this result, there is a significant change in the value of the confinement loss between the two refractive indices. Furthermore, at the analyte refractive index of 1.32 RIU, the peak confidence loss is 60.7 dB/cm at a wavelength of 580 nm. The wavelength sensitivity is obtained based on equation 4 of 1000 nm/RIU. The value of the analyte's refractive index was then increased to 1.33 and the confinement loss peak of 79.5 dB/cm was at a wavelength of 600 nm, so from 1.32 to 1.33 RIU, the refractive index had a sensitivity of 2000 nm/RIU. At the refractive index of 1.34 RIU, the confinement loss peak is 104.6 dB/cm at a wavelength of 610 nm so the sensitivity is obtained at 1000 nm/RIU.

Figure 3 shows the shift of the confinement loss peak to changes in the analyte's refractive index. The proposed sensor has a wide sensing range from 1.3 – 1.34 RIU. Using equation 4 we can calculate the sensitivity obtained in this design, respectively for analytes with a refractive index of 1.3 to 1. 1.31, 131 to 1.32, 1.32 to 1.33, 1.34 to 1.35, 1.35 to 1.36, 1.36 to 1.37, 1.37 to 1.38 and 1.38 to 1.39 have sensitivities of 1000, 1000, 2000, 1000, 2000, 2000, 3000, 6000 and 12000 nm/RIU. The amplitude sensitivity (AS) obtained from the difference in CL for the two different indices can be seen in Fig. 4. It was found that the maximum AS in the range of refractive index 1.3 – 1.34 RIU was -146.63 RIU^{-1} at refractive index 1.34 RIU.

In the range of refractive index 1.35 – 1.38 RIU, the peak shift of the confinement loss is obtained as shown in Fig. 5. Amplitude sensitivity shows the performance of the sensor in measuring the analytical refractive index. Fig. 5 shows the shift of the design confidence loss peak to changes in the refractive index in the range of 1.35 – 1.39 RIU. When the analyte refractive index is 1.35 RIU, the design shows that the confinement is increasing and when it reaches the maximum height the confinement loss value decreases with wavelength and it is found that the confinement loss peak is at a wavelength of 630 nm. At 660 nm the confinement loss value continues to increase until the design can only detect analytes with a refractive index of 1.39 RIU with a confinement loss value of and at a wavelength of 870 nm. This design cannot detect analytes with a refractive index of 1.4 and so on. This result occurs because the

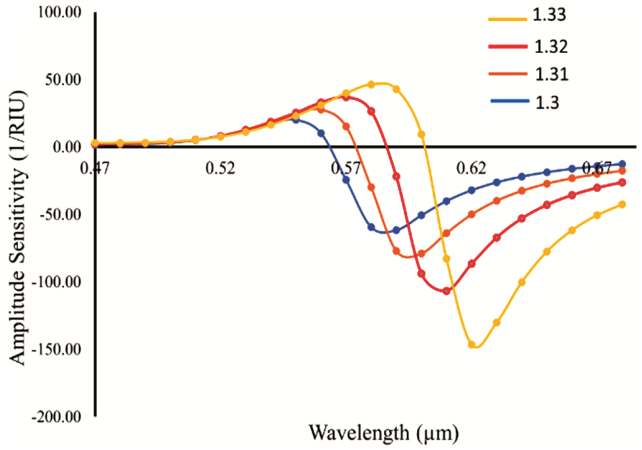

Fig. 4 — Amplitude sensitivity PCF-SPR in the range 1.3 – 1.34 RIU.

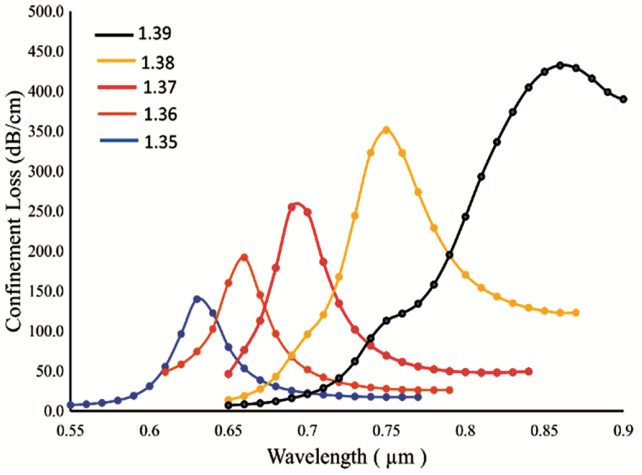

Fig. 5 — Confinement loss peak shift to changes in refractive index 1.35-1.38 RIU.

analyte with a refractive index of 1.4 did not find x-pol in the effective refractive index of this design, nor was a resonance wavelength found in this design. As shown in Fig. 5. Furthermore, a performance analysis was carried out on this refractive index range by obtaining the sensitivity amplitude as shown in Fig. 6. In the range of refractive indexes 1.35, 1.36, 1.36, 1.37, 1.37 and 1.38 RIU, meanwhile, the sensitivity amplitude was not found in the index. biased 1.38 and 1.39 RIU.

Amplitude sensitivity shows a shift in the value of 1/RIU negative which will shift along with changes in the refractive index of the analyte. Furthermore, a performance analysis is carried out on the design by determining the peak confinement loss for each change in the refractive index which can be shown in Fig. 7. The confinement loss peak always increases with the increase in the value of the analyte refractive index. The confinement loss value of each analyte is in the refractive index of 39.3 to 432.6 dB/cm. Further, the performance factor of the proposed sensor is shown in Table 1 and The proposed sensor has better performance than the previously proposed sensor design, as in Table 2

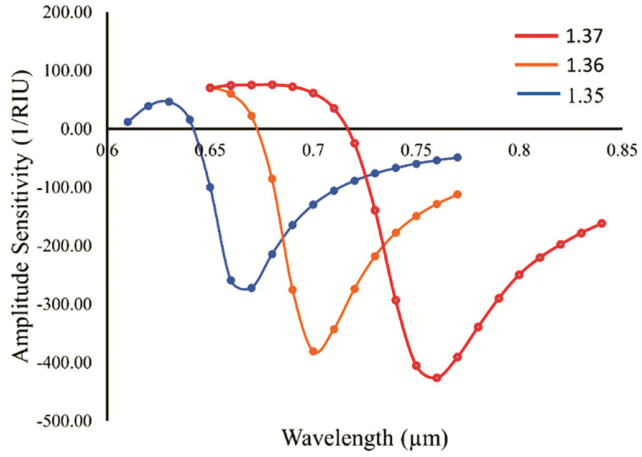

Fig. 6 — Amplitude sensitivity sensor design in the range 1.35-1.38 RIU.

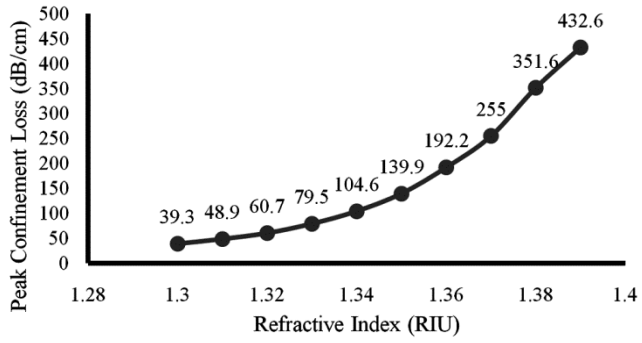

Fig. 7 — Shift of the confinement loss peak to changes in refractive index.

3.2 Effect of gold thickness on sensor performance

The effect of gold thickness is evaluated in this design based on the confinement loss value of each gold thickness. In the design, the gold thickness was varied by 30 nm, 35 nm, and 40 nm. The confinement loss values can be shown in Fig. 8 S-PCF-SPR with 30 nm, 35 nm, and 40 nm gold layers, the confinement loss peaks are at the same wavelength, namely 660 nm. Meanwhile, the peak confinement loss values were 414 dB/cm, 324 dB/cm, and 192.2 dB/cm, respectively. shows that the thicker the gold layer, the smaller the confinement loss value

Table 1 — Proposed sensor performance factors

na (RIU)	Peak Loss (dB/cm)	WS (nm/RIU)	AS (1/RIU)
1.3	39.3	-	
1.31	48.9	1000	-61.7
1.32	60.7	1000	-79
1.33	79.5	2000	-106.7
1.34	104.6	1000	-146.63
1.35	140	1000	-272.3
1.36	192.2	3000	-380.7
1.37	255	3000	-426.23
1.38	351.6	6000	-
1.39	429.3	12000	-

Table 2 — Comparison with other design

Reference	RI range	Maximum WS (nm/RIU)	Resolution (RIU^{-1})
[40]	1.35-1.4	3330	-
[41]	1.4 – 1.46	3000	$3.33\ 10^{-5}$
[42]	1.25-1.3	1932	$3\ 10^{-5}$
[43]	1.38 – 1.41	4100	$2.44\ 10^{-5}$
[44]	1.33-1.34	1371	-
[45]	1.33-1.40	12000	-
Purposed Sensor	1.30 – 1.39	12000	$5.4\ 10^{-5}$

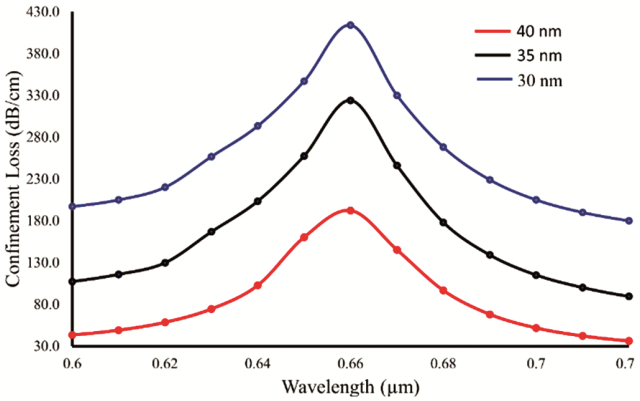

Fig. 8 — Effect of gold thickness on component confinement loss.

generated in this design. The thickness of the gold film has a great impact on the sensing performance. If the gold layer is too thick, the sensitivity and peak confinement loss will be significantly reduced, because the electric field cannot penetrate the gold layer. Meanwhile, if the gold layer is too thin, the plasmonic waves will be strongly damped due to radiation attenuation.

3.3 Effect of distance between holes on sensor performance

In this section, the PCF-SPR confinement loss values are evaluated for different hole distances, the hole distances being varied are 1.6 µm, 1.7 µm, and 1.8 µm. The refractive index of the analyte used in this section is 1.36 RIU and the component loss confinement is obtained as shown in Fig. 9. It is shown that the larger the size of the design profile and the greater the distance between the holes, the smaller the confinement loss value as well as the best, peak value of the confinement loss between each distance. holes 1.6 µm, 1.7 µm, 1.8 µm are 109.4 µm, 192.2 µm and 54.9 µm. and are known to be at wavelengths of 660 nm, 660 nm, and 670 nm, respectively.

3.4 Effect of hole size on sensor performance

In this sub-material, the PCF-SPR design is evaluated according to the size of the surrounding air holes. Variations in the size of the air holes tested in this section are air holes with diameters of 1.2 µm, 1.3 µm, and 1.4 µm. Variations in air hole diameter were compared based on the PCF-SPR confinement loss. From the simulation results, the relationship between confinement loss and air diameter is obtained as shown in Fig. 10

In this section, we identify the effect of PCF-SPR hole size on the confinement loss peak. The refractive index of the analyte used in this section is 1.36 RIU and the air hole spacing is 1.7 µm. It was found that the peak of the resonance wavelength was at a wavelength of 660 nm. It was found that the small size gives a very large confinement loss value as shown in Fig. 10. At the 1.2 µm hole diameter size the maximum confinement loss value is 1140.3 dB/cm, then at the hole size of 1.3 µm, the confinement loss value is 493.4 dB/cm, and finally at hole size 1.4 µm, the confinement loss peak is 192.2 dB/cm. From this data, an inverse relationship is obtained between the size of the air hole in the design and the confinement loss value. High confinement loss will give a high signal loss value also for fabricated PCF-SPR.

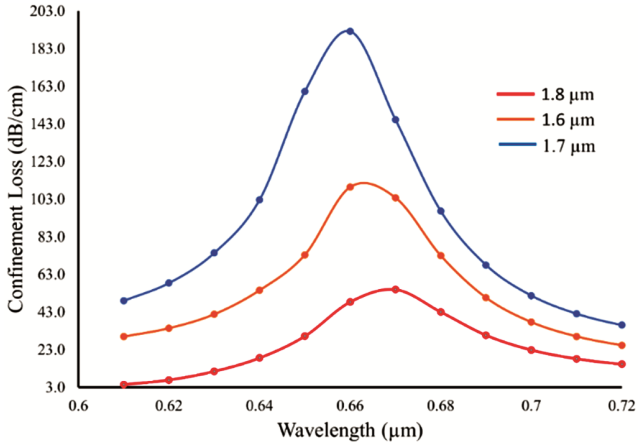

Fig. 9 — Effect of distance between wholes on confinement loss.

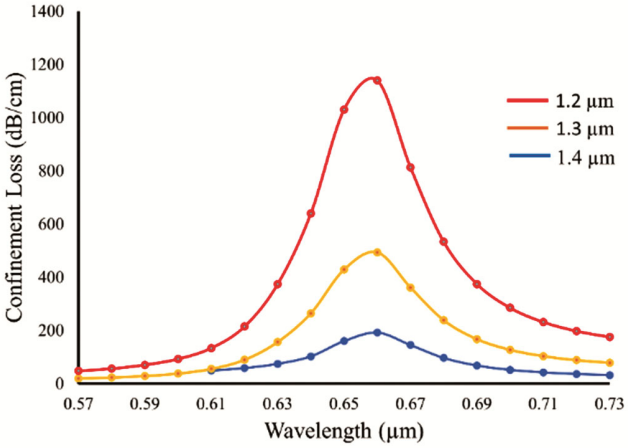

Fig. 10 — Effect of hole size on the confinement loss of the S-PCP-SPR component.

4 Conclusions

S-PCF-SPR sensor simulation has been carried out using the finite element method based on COMSOL Multiphysics version 5.6. The sensor is coated with a layer of gold with a thickness of 40 nm, and the material used is fused silica. After the simulation, it was found that this sensor can detect the refractive index in the range of 1.3 - 1.39 RIU, this result is better when compared to previous studies. Performance tests were also carried out on the sensor to detect the refractive index, and it was found that the sensor is ultra-sensitive with a sensitivity value of 12,000 nm/RIU. besides that, the sensor resolution is obtained at 5.4 x 10^{-5}. The effect of gold layer thickness was also tested with this sensor design and it was found that a thick gold layer gives a small confinement loss value, this is due to the presence of an electric field that cannot penetrate the gold layer. It

was also found that the resonant wavelength increased followed by an increase in the refractive index. This sensor can be used in biomedical or biochemical fields to detect cancer cell analytes.

Acknowledgments

We would like to thank LPPM Universitas Riau for their great support in this research under DRTPM Desentralisasi with contract no. 1643/UN19.5.1.3/ PT.01.03/2022. We also would like to thank the head of the Optoelectronic Laboratory at the University of Riau and the BRIN Physics Research Center for facilitating research activities.

References

1 Li X, Gong P, Zhao Q, Zhou X, Zhang Y & Zhao Y, *Sens Actuators B Chem*, 359 (2022).
2 Yin Z, Jing X, Zhang H, Wang C, Liu C & Shao P, *Optik (Stuttg)*, 262 (2022) 169320.
3 Haque E, Noman A A, Hossain M A, Hai N H, Namihira Y & Ahmed F, *IEEE Photon J,* 13 (2021) 1.
4 Singh S & Prajapati Y K, *Optik (Stuttg),* 235 (2021).
5 Feng Y, Li H, Li S, Liu Y & Meng X, *Sensors*, 21 (2021) 21.
6 Mo X, Lv J, Liu Q, Jiang X & Si G, *Sensors*, 21 (2021) 18.
7 Saad Y, Selmi M, Gazzah M H & Belmabrouk H, *Eur Phys J Plus*, 136 (2021) 5.
8 Yang X, Wang Z, Liu Y & Yao J, *Opt Mater Express*, 11 (2021) 2468.
9 Liu L, Zheng J, Deng S, Yuan L & Teng C, *IEEE Trans Instrum Meas*, 70 (2021).
10 N Luan, *et al.*, *IEEE Photon J,* 14 (2022) 3.
11 S Gu, *et al.*, *Optik (Stuttg),* 259 (2022).
12 Li B, Zhang F, Yan X, Zhang X, Wang F & Cheng T, *IEEE Trans Instrum Meas*, 71 (2022).
13 Teng C, *et al.*, *IEEE Sens J*, 22 (2022) 7.
14 Han B, *et al.*, *Opt Laser Technol*, 113 (2019).
15 Pan F, Zhang A, Pan H & Cao C, *J Mod Opt*, 69 (2022).
16 Dash J N & Jha R, *Plasmonics*, 11 (2016).
17 Islam M R, *et al.*, *Optik (Stuttg),* 221 (2020).
18 Bing P, Li Z Y, Yao J Q, Lu Y, Di Z G & Yan X, *Optoelectron Lett*, 8 (2012).
19 Shakya A K, Ramola A, Singh S & Van V, *Opt Express*, 30 (2022).
20 Chen J, Hou S & Lei J, *Jpn J Appl Phys*, 60 (2021).
21 Ramola A, Marwaha A & Singh S, *Appl Phys A Mater Sci Process*, 127 (2021).
22 Yasli A, *Plasmonics*, 16 (2021).
23 Islam M R, *et al., Appl Phys A Mater Sci Process*, 127 (2021).
24 Islam M R, *et al.*, *Opt Quant Electron*, 53 (2021).
25 Sakib M N, *et al.*, *Results Phys,* 15 (2019).
26 Lu Y, Wang M T, Hao C J, Zhao Z Q & Yao J Q, *IEEE Photon J*, 6 (2014).
27 Rifat A A, *et al.*, *IEEE Photon J*, 8 (2016).
28 Singh S & Prajapati Y K, *Optik (Stuttg),* 224 (2020).
29 Abdulrazak L F, *et al.*, *Opt Quant Electron*, 54 (2022).
30 Otupiri R, Akowuah E K & Haxha S, *Opt Express*, 23 (2015).
31 Kamrunnahar Q M, *et al.*, *Nanomaterials*, 12 (2022).
32 Rahman K M M, Alam M S & Islam M A, *IEEE Sens J*, 21 (2021).
33 Haider F, *et al.*, *IEEE Trans Nanobiosci*, 21 (2022).
34 Han H, *et al.*, *Sensors(Switzerland)*, 20 (2020).
35 Hossain M B, *et al.*, *Results Phys,* 18 (2020).
36 Paul B K & Ahmed K, *Opt Fiber Technol*, 53 (2019).
37 M. S. Islam *et al.*, *Appl. Opt*, 57(2018).
38 Abdullah-Al-Shafi M & Sen S, *Sens Bio-Sensing Res*, 29 (2020).
39 Tahhan S R & Taha R M, *Sens Bio-Sens Res*, 35 (2022).
40 Meng F, Wang H & Fang D, *IEEE Photon J*, (14) 2022.
41 Danlard I, Mensah I O & Akowuah E K, *Optik (Stuttg)*, 258 (2022).
42 Kumar D, Sharma M & Singh V, *Mater Today Proc*, (2022).
43 Bahloul L, Ferhat M L, Haddouche I & Cherbi L, *J Opt*, 51 (2022).
44 Zhang Y, *et al.*, *Mater Res Express*, 8 (2021).
45 Al-Mahfuz M, *et al.*, *Opt Mater(Amst)*, 90 (2019).